Sentinel-1 Radar Interferometry Applications

Francesco De Zan,   DEI – POLIMI, Italy
Andrea Monti Guarnieri,   DEI – POLIMI, Italy
Fabio Rocca,   DEI – POLIMI, Italy
Stefano Tebaldini,   DEI – POLIMI, Italy

Abstract

The short revisit time in the ERS Tandem experiment shows the data quality reachable when the temporal coherence is high. Sentinel 1 [5] will have a revisit time of 12 days. Using the 3 days repeat data from the ice phase of ERS1, we evaluated the improvements for distributed scatterers interferometry. Slow ground motion, visible in many successive images, allows the estimation of the subsidence rate from the interferogram stacks and not only from Persistent Scatterers. Interferograms at multiple spans can be optimally combined. The dispersion of the subsidence rate estimate obtained in one year using interferogram stacks compares favourably to a PS, if the number of pixels used is greater than say 100. We compare the Cramér Rao bound for the subsidence estimates for a Markov model of the temporal decorrelation to an approximated optimal linear estimate found from the covariances of the interferograms at different spans. The unbiased subsidence rate estimates are consistent.

1 Exponential decorrelation: the fit

Many targets in a SAR image are not coherent over long temporal intervals, but nevertheless they can be exploited for motion estimation using "conventional" DInSAR techniques. Most approaches can be generally defined as *interferogram stacks* [2, 4]. We study target decorrelation for interferogram stacks, and provide a statistically consistent estimator, to be used mainly for the assessment of the ground motion accuracy. If we suppose that the time decorrelation mechanism is primarily due to the motion of the scatterers in the resolution cell [6] we can model this as a Brownian motion, or the sum of many successive independent and equally distributed motions. It is possible to substitute the variable describing motion in the line of sight with the variable describing the unwrapped phase because of the linear relation between the two. The decorrelation law is:

$$\gamma_n = \gamma_0 \rho^n; \quad \rho = \exp\left(-\frac{T}{\tau}\right); \tau = \frac{2}{\sigma^2}; \sigma = \frac{4\pi\sigma_{Bd}}{\lambda}$$

A Brownian motion in the look direction could have a standard deviation in a day of $\sigma_{Bd} = 1mm/\sqrt{(day)}$. This corresponds, for a single scatterer, to a time-constant $\tau = 40[days]$ in C-band. If the resolution cell contains many scatterers so that the observed reflectivity is the sum of elemental contributions, then the coherence shows the same exponential decay with time, provided that each element is affected by the same independent Brownian motion. An alternative Markov model making the assumption that the elemental scatterers in the resolution cell change at random but suddenly the reflectivity leads to the same exponential decorrelation.

1.1 Validation with real data

The results here discussed are based on scenes from an ERS-1 Ice-Phase data set (Track 22, Frame 2763) acquired over central Italy. During this acquisition phase, the revisit interval was 3 days. The images were range over sampled 2:1 and co-registered. A portion of the scene was then selected (20×15km, range× azimuth). It is near the Fiumicino (Rome) airport and shows the last part of course of the Tevere river [6]. We studied the decorrelation dynamics for the time span of a few weeks. We worked with a reduced set of 17 images in the range ±250m (B_{perp}).
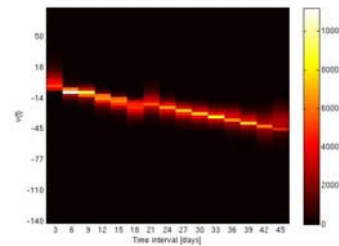
Figure 1 Histogram of the log coherences (best 60%) versus span

We applied a spectral shift filtering in the common band and spatially averaged on windows of 12×12 pixels (range over sampled 2:1). For each window, we L1 fitted an exponential decay with variable initial coherence γ_0 and time constant τ. The histograms of these two parameters are presented in [6]. The average time constant is about 40 days. In figure 1 we show the histogram of the 60% best fitting log-coherences as a function of the time span of the interferogram, after rescaling with respect to the time constant and the initial coherence. The histogram is centered on the line with slope -1, as in the exponential model.

Implication for 12 day repeat pass

Making use of the above model we can predict the coherence for a given time span and compare it to the 12 day coherence from that measured from the dataset. A typical value we would expect is 0.4-0.5. A change in the revisit time impacts on resolution (larger swaths imply coarser azimuth resolution) and number of available interferograms. These two effects broadly compensate: more interferograms means more samples in time, coarser resolution means less samples in space. However, for caution, we neglect the increase of interferograms and consider only spatial averaging to improve the interferogram quality. Moreover, the Sentinel-1 system shortens the revisit time to 12 days without reducing the final resolution, thanks to the augmented system bandwidth [5]. The big difference is in the temporal decorrelation for which we have to consider the combined effect of γ_0 and τ. The Cramér Rao bound for the phase variance gives the well known expression [1]:

$$\sigma_\phi^2 \leq \left(1 - \gamma^2\right) / \left(2\gamma^2 L\right)$$

with L being the number of independent samples averaged. With the exponential model of coherence, the expected dispersion of the interferometric phase for a wide variation of γ_0 from 0.3 to 0.7 increases 4-5dB moving from 12 to 35 days. Conversely, operating Sentinel-1 with a halved spatial resolution in order to bring the revisit time to 6 days, we lose 1-2dB as the increased temporal coherence does not compensate the resolution degradation.

2   The model for the distributed scatterers

Starting from the results presented in the previous section, we introduce the model to be used for the distributed scatter. The input is a distributed target made by L independent samples, subject all to the same subsidence and decorrelation. The index n is the discrete time at which the acquisition has been made, and the scene decorrelation comes out from the *AR(1)* model, so far discussed, i.e. a white source u_n that feeds a single pole filter. For the GS1 case we will assume the pole equal to:

$$\gamma_{nm} = \gamma_0 \rho^{|n-m|}; \ \rho = 0.74$$

The pole is modulated by the subsidence rate. White noise n_n, to be added, accounts for the other target decorrelation sources. The L pixels phases can be averaged to get a single "super-pixel" with an SNR increased by a factor L. Finally, the Atmospheric Phase Screen [3] due to the water vapor, adds to each image a white phase noise, a_n that is identical on all the L looks as long as their mutual distance is not greater than say 500m. In this term, we can include also the target elevation error contribution.

2.1.2   DInSAR Subsidence rate estimate

The optimal estimation of the subsidence rate, v, is complicated by the presence of target decorrelation, additive noise (clutter and thermal) and multiplicative noise (APS). In particular, this last contribution makes the PDF of the observations non- Gaussian. As a matter of fact, we have observed that in literature most of the "interferogram stacking" techniques are heuristic combinations of interferograms weighted according to a mixture of coherence and temporal baseline.

We will derive a bound for the estimate of the subsidence rate and we will define a suitable DInSAR-based estimate. We approach the problem here by approximating the APS phase screen as an additive noise. Moreover, we assume large SNR, that is $L>>1$, and relatively large scene coherence, say $\gamma>0.5$, that allows us a simple derivation of the ML estimate of the subsidence rate as well as its Cramér-Rao Bound.

An exact ML estimate can be derived by a more refined statistical analysis. This has been done in [7], splitting the problem of estimating the subsidence rate in a two steps, where first the interferometric phases (including the APS) are retrieved as ML estimate from the complex images, and then the subsidence rate is retrieved from the phase series. This approach, that cascades two optimal estimates, is not overall optimal in strict statistic sense, but it is likely to be close.

In the other approach [6], the model is linearized and the subsidence rate is estimated in one shot. The results achieved by the three different approaches have been compared: although the estimators are different, they fit very well one against the other, and get close to the value that we find in simulations.

2.2   Simplified spectral properties

We consider a fixed pixel, so that APS and thermal+clutter merges in a single, white noise added to the take and we account later for the averaging over L samples. The contribution of temporal decorrelation to the interferogram n,m is related directly to the *AR(1)* parameters. The center frequency of the power spectrum depends on the subsidence rate. We can thus estimate v in the frequency domain. Moving to the DFT:

$$Z_k = \sum_{n=0}^{N-1} z_n \exp\left(-j\frac{kn}{N}\right)$$

we see that Z_k is a nonstationary, incorrelated, zero-mean, Gaussian circular process. Its likelihood is:

$$p(\mathbf{Z} \mid \phi) = \frac{1}{|\mathbf{C}|} \exp\left(-\frac{\mathbf{Z}^* \mathbf{C}^{-1} \mathbf{Z}}{2}\right)$$

and the covariance matrix is diagonal, its elements being the power spectrum. The log-likelihood is thus blind with respect to the source phase and information

on v is contained in the location of the peak of the PSD. The ML estimator is the maximizer ψ of the average power of the whitened spectrum:

$$\hat{\phi} = \arg\max_{\psi}\left(-\sum_{k=0}^{N-1}\frac{|Z_k|^2}{S_k}\right)$$

where the S_k are the power spectral density elements of the sequence z_n. The spectral analysis allows us to provide an alternative formulation of the ML. We can in fact compute the periodogram by applying the DFT to the sampled estimate of the process and taking the modulus, or transforming the autocorrelation. The two formulations lead to two approaches in the ML estimate: 1. apply a proper weighting to the N images (i.e., the DFT), take the squared amplitude $|Z_k|^2$, then estimate v by the ML; 2. Compute all the *N(N-1)/2* interferograms, and perform the proper weighting - the DFT operator and then implement the ML estimate. The two approaches correspond to [6][7]: although in the end they get similar results, they are difficult to compare. The whitening operation could be performed in the time domain simply for an *AR(1)* model (no noise). The perfect whitening is achieved by the 2-samples FIR:

$$H_w(z) = 1 - \rho\exp(j\phi)z^{-1}$$

This allows us to interpret the subsidence rate as the phase of the average of the interferograms taken at the shortest span (12 days), or identically, as the argument of the first sample of the autocorrelation estimate. If the thermal, clutter and atmospheric noises add up, we have a filling of the spectrum, that can no longer be deconvolved by a simple 2-samples operator. We need many more spans, or a higher order whitening. We can for example truncate to an order M the autocorrelation sequence and compute the whitening operator by identifying the *AR(M)* process, e.g. by inverting the Yule-Walker equations. In [5] the estimate of the velocity rate is provided as a function of the interferograms at all the spans.

3. Cramér-Rao Bound

The Cramér Rao Bound for the rate estimate is derived by exploiting the log likelihood. The expression leads to the simple interpretation that the most relevant spectral contributions are those with a high derivative and a low power (noise floor). We remember that the spectra are circular. The spectrum can be evaluated either as a convolution of the spectrum and the DFT squared of the window or as the DFT of the windowed autocorrelation. We approach two different cases: (1) the window size is so large that the convolution does not affect appreciably the evaluation of the CRB, or (2) the window size is so small that dominates the performances. For a rough value of *N,* we observe that as the autocorrelation decades as *0.74^n*, so its lag *p=7* is *10dB* lower than lag *p=0*. We expect this to be the case when *N = 30* (yearly takes). We have then, if centered on v=0;

$$S(\phi) = \frac{N\sigma_u^2}{1 + \rho^2 - 2\rho\cos\phi} + N\sigma_n^2$$

This expression is not suited for a closed form solution, and can be integrated numerically to derive the CRB. Ignoring clutter and atmospheric noise, we get a lower bound for the subsidence rate when affected only by temporal decorrelation. Converting into subsidence rate variance, we have to average on the *L* looks times *N-1* interferograms. We expect the best accuracy, but thermal and atmospheric noises leads to higher variances.

$$\sigma_v^2 = \frac{1-\rho^2}{2(N-1)L\rho^2}\left(\frac{\lambda}{4\pi\Delta T}\right)^2$$

With added noise, the best results need more interferogram spans: longer delays see greater phase shifts, but the coherence is lower. For *N* small, the PSD of the *AR(1) + noise* process is to be convolved with a window whose lobe is quite large. The resulting spectrum is quite smooth, and the variance of the estimate is worsened. Loosely speaking, we can approximate the PSD of the *AR(1) process + noise* as a the PSD of a complex sinusoid (whose frequency is the subsidence rate) plus noise, and this approximation holds as far as the main lobe of the AR is small compared with the window bandwidth 1/N. In this case, we expect that the accuracy of subsidence rate estimation is approximated by the N^{-3} (N small, remember) power law found for a PS.

4. Rate error budget estimate

The analysis of DInSAR allows us to define an approximation, depending in particular on *N, L, ρ,* the APS phase noise variance, and the thermal, clutter and volumetric decorrelation. This variance of the estimate of velocity is the combination of two contributions. When the number of image spans a time interval shorter than the decay time of the coherence, there is no relevant difference between the spectral properties of the *AR(1)* and the PS case. The rate error has the same expression that holds for PS.

$$\sigma_v^2 = \left(\frac{\lambda\sigma_t}{4\pi T}\right)^2\frac{12}{N^3 - N}$$

and σ_t is the variance of the travel path due to the APS. Notice that the error rate variance decreases with N^3, as for the PS case. When the number of images becomes large, and longer than the time decay of the coherence, the temporal decorrelation becomes more and more influent, leading to the lower bound seen before. In absence of APS, clutter and thermal noise, it predicts a decrease of the variance according to N. The actual behavior of the variance may be qualitatively modeled as a mixture of the two. A plot of this behavior is given in Fig. 2. The figure has been computed by assuming conditions very close to those

for PS interferometry. The scene short term coherence was assumed 0.6. If we exploit the combination of interferograms taken at T = 12 days, the overall coherence of each interferogram, including temporal decorrelation, would be $\gamma = 0.4$. The contribution of the APS is still dominating, leading to a rate error of 3.4 mm/year. This result is worse than in the actual PS case since then it is possible remove the APS by estimating it in each image. Notice that $L = 30$ looks of 100 m^2 each would correspond to about 200 measures in the APS lobe, in the best case, but less in practice, given the sparsely coherent DInSAR pixels. But it may be possible to separate within an APS lobe the contributions of the areas where we expect to have no subsidence, in order to estimate and abate the APS itself. Finally, notice that the floor provided by the AR model is very close, at 2.9 mm/year. A further increase in the number of acquisitions would not lead to a significant improvement, a part from that of adding an independent measure (so a factor $N^{-1/2}$). Second, increasing the number of looks would not change too much the result, as it would not affect the APS error. Therefore, we can conclude that the plot represents a good possible balance between different and contrasting effects. An interesting conclusion drawn in [6] is that the exponential model of the coherence, so nicely fitting in Figure 1, implies a substantial uniformity of the behavior of the subsidence rate estimate with frequency, at least in the interval between 1.5 and 6 GHz.

5. Conclusion

An evaluation of the subsidence rate error budget has been carried out for DInSAR interferometry, using the 3 days revisit interval data over Rome taken by ERS - 1. The results of modeling temporal decorrelation with a Brownian motion depend upon the number N of images used and the revisit interval T. Assuming a short term target coherence of 0.6 and averaging measures over L=100 independent looks the dispersion of the velocity estimate is lower than 4 - 4.5 *mm/year* for a 12 days revisit time.
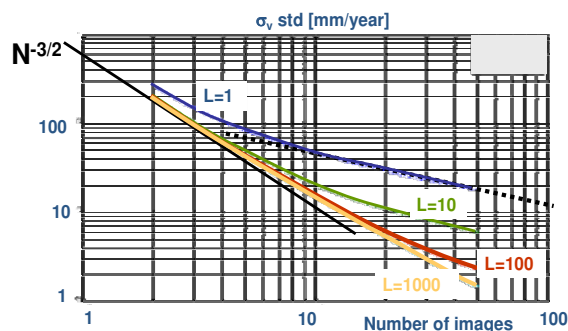
Figure 2   Accuracy in the estimate of the subsidence rate in *mm/year* using interferogram stacks on *L* pixels undergoing the same atmospheric disturbance. *N* is the number of images, taken at 12 days interval. The black line reports the behavior of a single PS.

References

[1] R. Bamler and P. Hartl. SAR interferometry. Inverse Problems, 14, R1-54 , 1998.

[2] Y. Fialko. Interseismic strain accumulation and the earthquake potential on the southern S. Andreas fault system. Nature, 441:968--971, 2006.

[3] R. Hanssen. Radar Interferometry: Data Interpretation and Error Analysis. Kluwer Academic Publishers, Dordrecht, 2001.

[4] A. Hooper, H. Zebker, P. Segall, B. Kampes, A new method for measuring deformation on volcanoes and other natural terrains using ISAR persistent scatterers, Geoph. Res. Letters, 31

[5] Mission Requirement Document, Sentinel - 1 http://esamultimedia.esa.int/docs/

[6] F. Rocca, Modeling Interferogram Stacks, IEEE Trans. on Geoscience and Remote Sensing, Vol. 45., N. 10, Oct 2007, pp 3289 - 3299, 2007

[7] S. Tebaldini and A. Monti Guarnieri, Hybrid Cramér-Rao Bounds for Crustal Displacement Field Estimators in SAR Interferometry,   IEEE Signal Processing Letters, to be published.

[8] H. A Zebker and J. Villasenor. Decorrelation in interferometric radar echoes. IEEE Transactions on Geoscience and Remote Sensing, 30(5):950--959, September 1992.